PAPER

First-principles insights into sulfur and nitrogen co-doped Ti$_2$CO$_2$ MXene as an advanced anchoring material for sodium polysulfides in sodium–sulfur batteries

Nguyen Van Nghia,[a] Trinh Thu Bien,[b] Nguyen Truong Long [iD][b]
and Minh Triet Dang [iD] *[b]

Room-temperature sodium–sulfur (Na–S) batteries have attracted significant attention for large-scale energy storage due to their high energy density, environmental compatibility, and cost-effectiveness. Nevertheless, their practical application is severely hindered by the shuttle effect resulting from the dissolution of sodium polysulfides into electrolyte solvents and the intrinsically poor conductivity of sulfur cathodes. In this work, we systematically investigate, by first-principles density functional theory calculations, the effectiveness of doping sulfur (S) and co-doping nitrogen (N) and sulfur (S) atoms on Ti$_2$CO$_2$ MXene as anchoring materials for sodium polysulfides (Na$_2$S$_x$). Our results indicate that both doping and co-doping significantly enhance the adsorption strength of Na$_2$S$_x$ clusters on Ti$_2$CO$_2$ surfaces compared to pristine MXene, with the NS co-doped Ti$_2$CO$_2$ exhibiting the strongest adsorption ability, especially for high-order polysulfides (Na$_2$S$_6$, Na$_2$S$_8$). We identify distinct adsorption mechanisms based on Bader charge analysis and projected density of states calculations, revealing substantial charge transfer from the adsorbed clusters to the MXene surface. Additionally, doping with S and NS co-doping significantly enhances electronic conductivity. Our findings offer theoretical insights into the beneficial role of heteroatom doping in MXenes and highlight NS co-doped Ti$_2$CO$_2$ as a promising candidate for mitigating polysulfide shuttle effects in next-generation Na–S batteries.

1. Introduction

Since the commercialization of lithium-ion (Li-ion) batteries by Sony Corporation about three decades ago,[1] these rechargeable batteries have become indispensable for portable electronic devices and electric vehicles due to their superior energy density, lightweight construction, and long cycle life. However, limited lithium reserves and approaching the theoretical threshold of energy density for Li-ion batteries have sparked extensive efforts to explore alternative battery technologies beyond lithium.[2–5] Among promising candidates, room-temperature sodium–sulfur (Na–S) batteries have gained considerable attention as potential replacements for Li-ion batteries, offering high theoretical energy density (up to 1274 W h kg^{-1}),[6,7] economical price and natural abundance of sodium compared to lithium, multi-electron transfer capability during charge–discharge processes due to sulfur redox chemistry, and lower toxicity.[7–10] Therefore, Na–S batteries possess

significant advantages of cost-effectiveness, environmental friendliness, and excellent electrochemical performance, making them highly attractive for next-generation energy storage applications. Despite these promising features, several critical challenges currently hinder the practical implementation of Na–S batteries. The primary obstacle is the notorious shuttle effect, arising from the dissolution of intermediate sodium polysulfides (Na$_2$S$_4$, Na$_2$S$_6$, Na$_2$S$_8$) into common electrolyte solvents during cycling.[11–15] These dissolved polysulfides migrate between the cathode and anode, causing severe self-discharge and rapid capacity fading, thus drastically reducing battery performance and lifespan. Additionally, the inherently low electronic conductivity of sulfur cathodes significantly limits the electrochemical kinetics of these batteries.[12–15] To counteract these problems, employing sulfur-host anchoring materials capable of strongly immobilizing sodium polysulfides and providing more charge transfer for higher electronic conductivity has emerged as a prominent strategy for enhancing battery performance.[16,17]

Recently, two-dimensional (2D) MXenes have been identified as excellent candidates for anchoring materials in Na–S batteries due to their large surface area, excellent electronic conductivity, abundant active sites, and tunable surface

[a]*Open Training Institute, Hanoi Architectural University, Km10, Nguyen Trai Street, Hanoi, Vietnam*

[b]*Can Tho University, 3-2 Road, Can Tho City 900000, Vietnam. E-mail: dmtriet@ctu.edu.vn*

chemistry, as demonstrated through extensive theoretical and experimental investigations.[18–21] To further enhance the polysulfide anchoring capabilities of MXenes and address the shuttle effect more effectively, surface modification *via* doping with heteroatoms has garnered considerable interest.[19,22,23] Such doping strategies have already been successfully implemented in other 2D materials, such as graphene and carbon nanotubes, by introducing heteroatoms (N, O, S, B), resulting in significantly strengthened interactions with lithium polysulfides in Li–S batteries.[24–26] Recent theoretical studies on MXenes have emphasized the role of surface doping with heteroatoms such as metals,[23] nitrogen (N),[27,28] and sulfur (S),[29] in tailoring electronic properties and enhancing polysulfide anchoring for Li- and Na-based batteries. For instance, N-doped porous Ti_3C_2 MXene has been synthesized and shown to improve electrocatalytic activity in Li–S batteries.[30] Density functional theory calculations indicate that nitrogen doping increases electron density at the surface, thereby enhancing Li atom adsorption and strengthening interfacial interactions with Li_2S clusters.[30] Further experimental investigations demonstrate that N-doped Ti_3C_2 MXene also exhibits excellent cycling stability, with a reversible capacity of 647 mAh g^{-1} after 650 cycles at 4 C and high sulfur loadings (3 and 6 mg cm^{-2}), confirming its suitability as a sulfur host material.[31] Theoretical predictions also suggest that N-doped Ti_2CO_2 MXene transforms into a metallic state, offering a reduced diffusion barrier for Li ions and thereby enhancing ion transport.[28] In addition to nitrogen, sulfur has been explored as a dopant to improve MXene performance in both Na–S and Li–S batteries[32,33] as well as in Na/Li-ion battery electrodes.[34,35] Similar to nitrogen, sulfur doping enhances the electronic conductivity of pristine MXenes by increasing the density of states near the Fermi level.[33] For Na/Li-ion batteries, S-doped $Ti_3C_2O_2$ exhibits an enlarged interlayer spacing, increased surface area, and improved electrical conductivity, all of which contribute to faster ion transport, higher rate capability, and enhanced cycling performance.[34,35] For Na–S batteries, both theoretical and experimental results confirm the superior electrochemical performance of S-doped MXenes, with a reversible capacity of 577 mAh g^{-1} at 2 C sustained over 500 cycles.[32] More recently, co-doping with both nitrogen and sulfur has emerged as a strategy to combine the benefits of each dopant, producing MXenes with superior performance as sulfur hosts for Li–S and Na–S batteries.[23] These co-doped structures have been synthesized through annealing and solvothermal treatments, enabling their application in high-performance inkjet-printed micro-supercapacitors and nitrogen reduction electrocatalysis.[36,37] Co-doped NS-MXenes exhibit significantly improved gravimetric capacitance (495 F g^{-1} at 1 A g^{-1}), excellent rate capability (180 F g^{-1} at 10 A g^{-1}), and excellent cycle stability (98% retention over 6000 cycles) for Li-ion battery applications.[38] Mechanically, N-doping contributes to expanded interlayer spacing and elevated Ti valence states, while S-doping reduces ion diffusion barriers, collectively enhancing rate performance in these advanced MXene systems.[38] However, for Li–S and Na–S batteries, co-doping MXene surfaces with multiple heteroatoms to increase the number of active sites and further strengthen polysulfide

adsorption remains largely unexplored, particularly regarding the combined effects of nitrogen and sulfur doping. Given the individual potential of N and S atoms to enhance electronic properties and their strong interactions with sodium polysulfides, a systematic theoretical investigation of NS co-doped MXene could provide new insights into their adsorption mechanisms and significantly advance the development of Na–S battery cathodes.

In this study, we conduct a first-principles analysis of S-doped and NS co-doped Ti_2CO_2 Mxene to examine their modified structural and electronic properties and then explore their adsorption abilities with Na-polysulfides for applications in sodium-sulfur batteries. In Section 2, we describe our computational methods, which include density functional theory calculations, structural optimizations, and analyses of adsorption energies. In Section 3, we first examine the optimized geometric structures and electronic properties of S-doped and NS co-doped Ti_2CO_2 MXene. We then systematically analyze the adsorption mechanisms of sodium polysulfide (Na_2S_x) clusters on these doped surfaces, identifying distinct binding behaviors through Bader charge transfer and electronic structure analyses. We then summarize our findings and highlight the enhanced potential of NS co-doped Ti_2CO_2 MXene as an efficient anchoring material for practical applications in Na–S batteries.

2. Computational details

To study the adsorption of Na_2S_x clusters ($x = 1,2,4,6,8$) on our doped 2D layer Ti_2CO_2, we performed calculations based on density functional theory (DFT) *via* the Quantum Espresso package.[39] Our calculations employed PAW pseudopotentials[40] based on exchange-correlation functionals from Perdew–Burke–Ernzerhof[41] from the PS library.[42] The recently developed van der Waals interactions (vdW-DF3)[43,44] are also included. This functional of vdW-DF3 is selected due to its improved non-local correlation functional that can accurately describe dispersion interactions of physisorption of Na–S clusters with the 2D MXene surface. For Brillouin zone sampling, our Monkhorst–Pack k-grids[45] are $4 \times 4 \times 1$ and $8 \times 8 \times 1$ in structural optimization and electronic structure calculations, respectively. The energy cutoff is set at 60 Ry, while the convergence threshold in self-consistent field calculations is 10^{-8} eV, and the optimal force conditions are 10^{-4} eV Å^{-1}. Our study also performed additional calculations of DFT + U[46–48] for the electronic band structures and density of states. Our calculated electronic structure considered the Hubbard U correction for 3d shells of the titanium atoms, and the U value is selected at 3 eV based on ref. 49 and 50.

First, the two-dimensional pristine Ti_2CO_2 configuration is optimized with a supercell of $3 \times 3 \times 1$, and a vacuum space of 20 Å is used for 2D modeling to eliminate the effect of periodic images. Our optimized structure of pristine 2D MXene Ti_2CO_2 has the lattice constant at 2.979 Å, Ti–C bonding length at 2.163 Å, and Ti–O bonding length at 1.956 Å, in agreement with data from previous theoretical and experimental reports.[51–53] A model of doping S and co-doping N and S atoms is created by

replacing one or two O atoms on the surface with the doped atoms in several sites. Then, we optimized the model to find the most favorable energetic configuration. Several doped sites are examined for the doping atom to determine the most energetically favored site for doped atoms (Fig. S1 and Table S1). We found that the optimized models where the doped S or N atom replaces the O atom possess the lowest energy, in agreement with previous DFT calculations for S-doped and codoped NS on MXene.[32–34,36,37] The co-doping N and S atoms are positioned close to each other to explore co-doping synergistic effects between the two heteroatoms, which can enhance charge redistribution and adsorption behavior for Na–S clusters. The particle position of all these optimized configurations is presented in the SI. After obtaining the doped models, we examine the possible adsorption sites of the 2D structures and different rotations of Na_2S_x clusters on the surface of the doped MXene. The initial height of the Na_2S_x clusters on the top layer is set at 2.5 Å, and various adsorption sites are investigated to determine the lowest energy configuration. The adsorption energy (E_{ads}) of each cluster on 2D structures is calculated as:

$$E_{ads} = E_{cluster–MXene} - E_{cluster} - E_{MXene} \qquad (1)$$

where $E_{cluster–MXene}$ and E_{MXene} denote the total energies of the anchoring 2D materials with and without Na_2S_x clusters, respectively, and $E_{cluster}$ is the energy of the optimized Na_2S_x clusters. Only the best configuration corresponding to the lowest calculated energy for each absorbed Na_2S_x is reported and further analyzed. For analysis, the calculation of the Bader charge based on Henkelman's algorithm[54] via Critic2 (ref. 55) is

performed to explicitly quantify the charge transfer between the adsorbed sodium polysulfide and the doped MXenes. In addition, the charge density difference (CDD) is calculated as follows:

$$CDD = \rho_{cluster–MXene} - \rho_{cluster} - \rho_{MXene}$$

where $\rho_{cluster–MXene}$, $\rho_{cluster}$, and ρ_{MXene} represent the calculated charge densities in Na_2S_x adsorbed MXenes, isolated Na_2S_x clusters, and doped MXenes.

3. Results and discussion

3.1. Modified structure of S doping and co-doped S and N atoms on the surface of Ti_2CO_2 MXene

Optimized structures of two doped schemes of S-doping and N–S co-doping on the surface of 2D MXene Ti_2CO_2 are illustrated in Fig. 1. For S-doping, an S atom substitutes one O atom, and for co-doping, N and S atoms are substituted. The optimized energy configurations indicate that doped S and N atoms are located at the same sites as O atoms, but with different elevated heights on the termination O-plane. A similar result of the elevated height of S-doping compared to the unchanged height of substituted N-doping with an O atom on the surface is found in ref. 36. The doped S atom is located at a considerably higher height, at 0.66 Å, than the O-layer, while the doped N atom stays almost the same height as the O atom on the surface, with a difference of 0.02 Å. The Ti–S bond is elongated at 2.385 Å compared to the Ti–O bond at 1.956 Å, while the Ti–N bond is shortened at 1.908 Å.
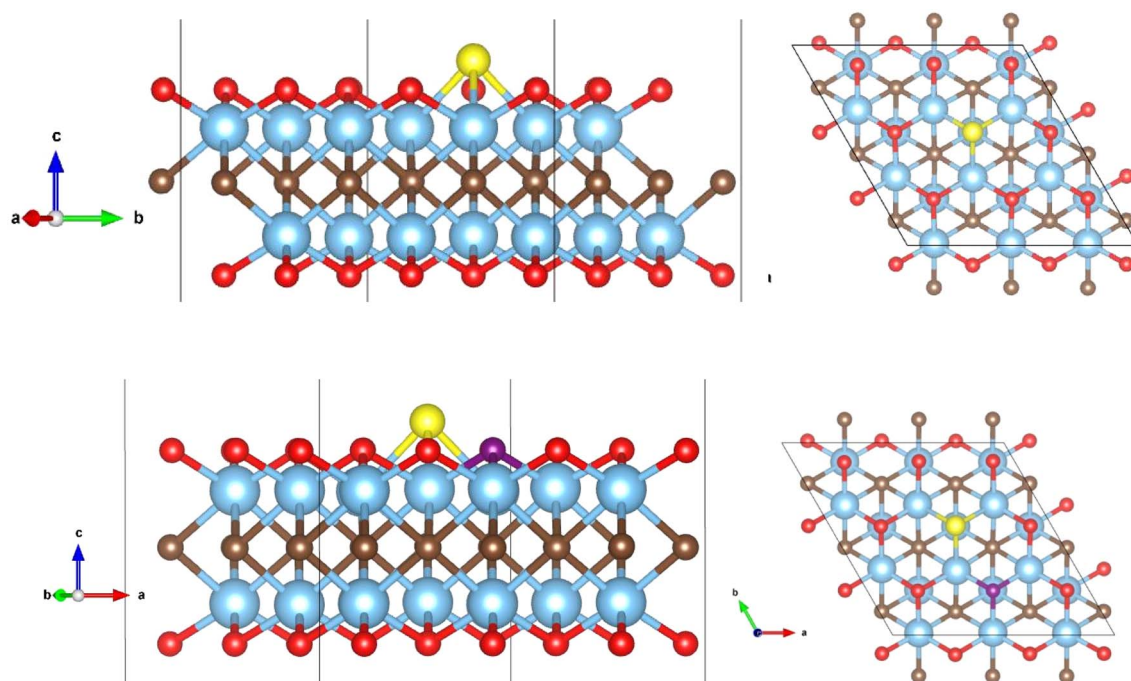

Fig. 1 (a) Top- and side-view of the optimized geometrical structures of doped S atom on the surface of 2D Ti_2CO_2 (b) top- and side-view of the optimized geometrical structures of co-doped N and S on the surface of 2D Ti_2CO_2. The light blue, red, brown, yellow, and purple spheres illustrate Ti, O, C, S, and N atoms, respectively.

The defect energy[34] is calculated *via* the difference in formation energy E^f of the doped S and co-doped N and S atoms on 2D Ti_2CO_2 using eqn (2):

$$E^f = E_{tot}[\text{doped } Ti_2CO_2] - E_{tot}[Ti_2CO_2] + n_i\mu_O - n_i\mu_{\text{doped atom}} \quad (2)$$

where $E_{tot}[\text{Doped } Ti_2CO_2]$ and $E_{tot}[Ti_2CO_2]$ are the total energies of the doped $Ti_2CO_2(S)$ or $Ti_2CO_2(NS)$ and pristine supercell Ti_2CO_2, respectively. μ_O and $\mu_{\text{doped atom}}$ (μ_S or μ_N) are basic elemental chemical potentials of O, S, and N atoms. These chemical potentials can be calculated as total energies per atom using DFT calculations. For details, the total energies per atom for μ_O, μ_S, and μ_N are obtained *via* DFT calculation of O_2 and N_2 molecules, as well as S_8 rings, isolated in a cubic cell.

The defect formation energy value is estimated at 2.49 eV for the doped S atom and at 3.43 eV for the N-doped scheme, while a higher defect formation energy for the co-doped scheme is found at 4.60 eV. The defect energy of co-doping S and N atoms is 4.60 eV, which is lower than the sum of defect energy at 5.92 eV for sole doping of S and N atoms (2.49 eV and 3.43 eV, respectively). This suggests that the S and N doping will attract each other on the surface of the MXene. This result for S-doping is in good agreement with the defect formation energy estimated at 2.31–2.47 eV of doping a S atom on a similar 2D MXene $Ti_3C_2O_2$.[34]

3.2. Adsorption of Na_2S_x clusters on $Ti_2CO_2(S)$ and $Ti_2CO_2(NS)$ MXenes

First, incorporating an S atom on the surface as active adsorption sites in Ti_2CO_2 MXene results in optimized adsorption sites, as shown in Fig. 2. The adsorption of Na_2S_x clusters with x = 1, 2, 4, 6, and 8 was focused since they are intermediates formed during the stepwise conversion of sulfur to Na_2S (*e.g.*, $Na_2S_8 \rightarrow Na_2S_6 \rightarrow Na_2S_4 \rightarrow Na_2S_2 \rightarrow Na_2S$) during the discharge/charge process in sodium–sulfur (Na–S) batteries.[56,57] All Na_2S_x clusters adsorbed on our MXenes retain their shapes relatively. Calculation of the change of total energy is performed to quantify the deformation of the cluster once anchored on our doped and co-doped MXenes in Table S2 in the SI. The difference in clusters' energy is from 0.009 to 0.126 eV per atom, indicating that the energy deformations are low. Therefore, the cluster's structural integrity will be preserved upon adsorption on our MXene. We found that the alignment of Na_2S_x clusters upon adsorption on the surface of $Ti_2CO_2(S)$ is similar to the adsorption of Ti_2CO_2 MXene and other 2D materials,[56,57] but expresses a strong attraction to the active site of the doped atom. While low-S content Na_2S_x clusters ($x = 1,2,4$) have both Na atoms bound toward or attracted closely to the doped atom, only one Na atom in high-S content clusters (Na_2S_6 and Na_2S_8) is bound to the doping atom. For the co-doped N and S model $Ti_2CO_2(NS)$ in Fig. 3, the alignment of high-content Na_2S_6 and Na_2S_8 clusters is different than the adsorption scheme of $Ti_2CO_2(S)$, Ti_2CO_2, and other MXenes.[21,57] Due to the presence of a second active site from the doped N atom, both Na atoms in Na_2S_6 and Na_2S_8 are bound to the surface, similar to the low-content clusters. We also found that the doped N atom only attracts the Na atom, while the doped S expresses affinity to both Na and S atoms in the sodium polysulfide clusters.

Fig. 4 demonstrates the binding ability of doped $Ti_2CO_2(S)$ and co-doped $Ti_2CO_2(NS)$ with Na_2S_x clusters *via* primarily calculated adsorption energies. For pristine MXene Ti_2CO_2, all clusters exhibit significantly greater adsorption energies than the binding energy with common electrolyte solvents (1,3-
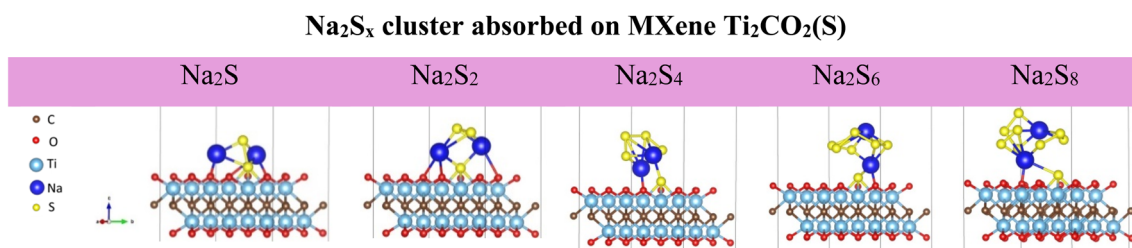
Na_2S_x cluster absorbed on MXene $Ti_2CO_2(S)$

Fig. 2 Optimized configurations of Na_2S_x adsorbed on doped $Ti_2CO_2(S)$ surface. The light blue, red, brown, yellow, and blue spheres illustrate Ti, O, C, S, and Na atoms, respectively.
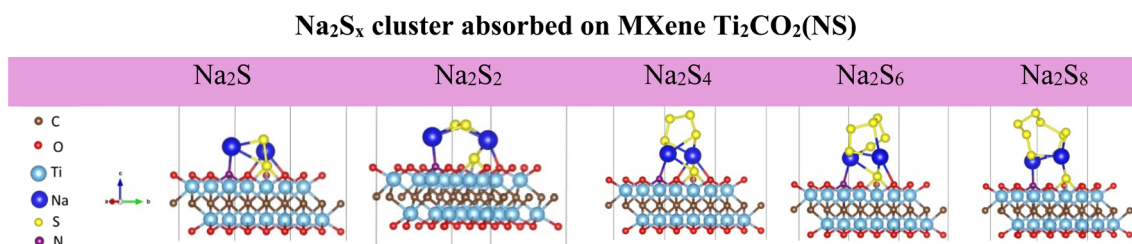
Na_2S_x cluster absorbed on MXene $Ti_2CO_2(NS)$

Fig. 3 Optimized configurations of Na_2S_x adsorbed on co-doped $Ti_2CO_2(NS)$ surface. The light blue, red, brown, yellow, purple, and blue spheres illustrate Ti, O, C, S, N, and Na atoms, respectively.
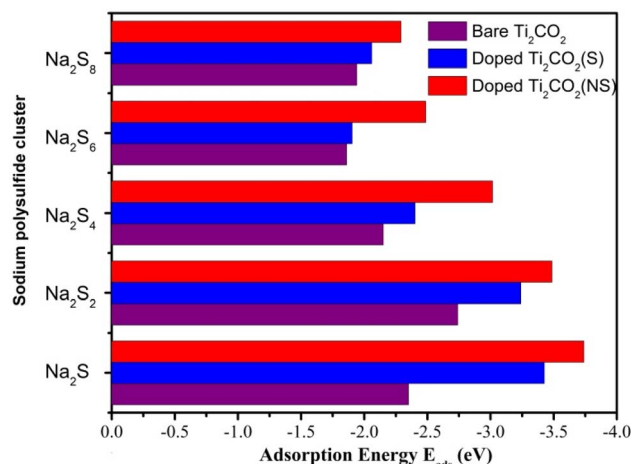
Fig. 4 Adsorption energies E_{ads} for Na$_2$S$_x$ clusters on doped Ti$_2$CO$_2$(S) and co-doped Ti$_2$CO$_2$(NS).

anchoring Na–S clusters. This result is consistent with other experimental and theoretical works in Li–S and Li-ion batteries. For example, S doping in mesoporous graphene microspheres helps immobilize and prevent the dissolution of Li-polysulfides.[26] Other doping schemes, such as N, B, and metal-dope, could be further developed as a clever strategy to enhance the binding of Li–S molecules in anchoring materials.[23,25,60] According to the analysis of these works, doping with N, S, and O atoms has a strong interfacial interaction with Li atoms. In contrast, B and P atoms have a stronger adsorption ability toward S atoms in the adsorption of Li–S clusters. Experimental doping N to porous MXene Ti$_3$C$_2$ has been proven to be an effective Li–S immobilizer and initiate a multifunctional electrocatalyst for the nucleation and decomposition of Li$_2$S in discharge and charge processes.[30] In this work, the calculation of N-doped Ti$_3$C$_2$ showed that the adsorption energy of the Li$_2$S cluster on the N-doped surface is higher than on the Ti$_3$C$_2$ surface by 0.05 eV. In our calculations for doping the S atom and co-doping N–S, the adsorption energies are greatly enhanced for Na$_2$S and Na$_2$S$_2$ clusters (from 0.50 eV to 1.39 eV), which is beneficial for improving the electrochemical reaction rates on the sulfur cathode. Notably, by introducing co-doped N and S, we can significantly enhance the adsorption capacity of high-S content Na$_2$S$_6$ and Na$_2$S$_8$ clusters, which remains weak in the pristine MXene.[12,21,57] Hence, aside from applications in Li-ion and Li–S batteries, S-doping and NS co-doping into MXene could have great potential for Na-ion and Na–S batteries.

The bond length of doped S and co-doped N and S with Na atom is illustrated in Fig. 5. For doped Ti$_2$CO$_2$(S), Na atom is bound to both the doped S atom and one O in the surface. The bonding of the O atom to Na is relatively intact upon the

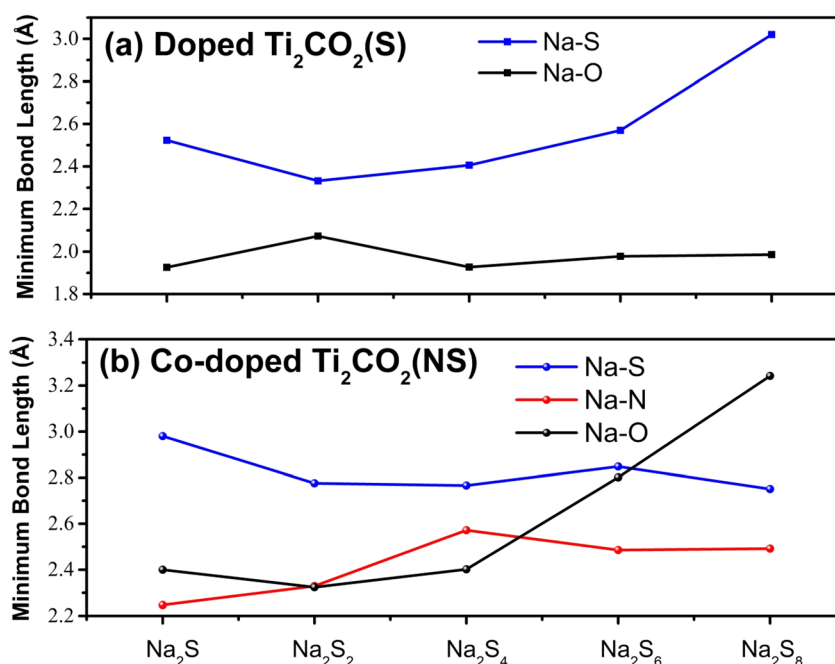dioxolane (DOL) and 1,2-dimethoxyethane (DME)), reported to be around −0.8 eV to −1.0 eV.[58,59] These values are approximately within the range of −1.94 to −2.74 eV, indicating that 2D Ti$_2$CO$_2$ MXene is a potential anchoring material. Moreover, this good binding ability could be enhanced by doping an S atom or co-doping N and S atoms. Fig. 4 indicates that all adsorption energies of Na$_2$S$_x$ clusters on S-doped Ti$_2$CO$_2$(S) are enhanced, ranging from 6.2% (Na$_2$S$_8$) to 37.2% (Na$_2$S). Meanwhile, all adsorption energies of Na$_2$S$_x$ clusters on co-doped Ti$_2$CO$_2$(NS) are promoted, ranging from 18.0% (Na$_2$S$_8$) to 59.0% (Na$_2$S). Therefore, the enhanced ability to capture sodium sulfide via doped S and co-doped N and S is significantly practical for

Fig. 5 (a) The minimum bond length of the Na atom to the doped atom S in doped Ti$_2$CO$_2$(S), (b) the minimum bond length of the Na atom to the doped atoms S and N in co-doped Ti$_2$CO$_2$(NS).

adsorption from low to high S-content clusters. However, the increased bond length of Na in higher S-content clusters with a doped S atom indicates that the doped S atom cannot anchor the Na atom as efficiently as in low-S-content clusters. On the other hand, in co-doped Ti_2CO_2(NS), the bonding of Na and the doped N atom is very short and increases slightly upon the adsorption of higher S-content clusters. Another difference is that the bond length of Na with doped S is maintained in both low and high-S-content clusters. This indicates the role of two doped atoms in higher S-content clusters, meaning that the bonding of the Na atom with the doping atoms of N and S is strong enough to anchor the Na–S cluster. In addition, extended distances of Na with O atom for adsorption of Na_2S_6 and Na_2S_8 clusters with co-doped Ti_2CO_2(NS) suggest that the O atom in the surface does not participate in the binding of high S-content clusters. This point in our adsorption of Na–S clusters collides with the previous discussion that doping with N or S atoms has a strong interfacial interaction with Li atoms in Li–S clusters.[25,60] It is also supported by the combined experimental and theoretical study on N-doped MXene, which shows that the doping atom, N, induces enhanced interfacial interaction with the Li atom in Li–S clusters.[30]
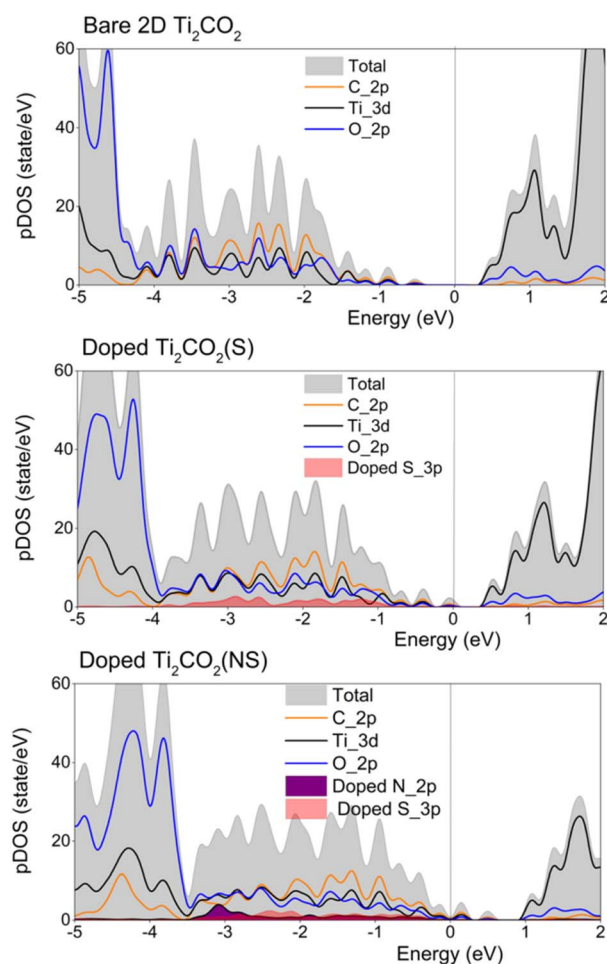

Fig. 6 Projected density of states (PDOS) of doped Ti_2CO_2(S) and co-doped Ti_2CO_2(NS) calculated by DFT + U. The Fermi level is set to zero and is indicated by the dashed lines.

3.3. Electronic structure upon adsorption of Na_2S_x clusters on undoped and doped MXenes

First, the effect of one doped S atom and co-doping S and N atoms on the termination layer of Ti_2CO_2 on the electronic structure of Ti_2CO_2 MXene is discussed in this section. We present the partial density-of-state (PDOS) of Ti_2CO_2 without and with doping of doped Ti_2CO_2(S) and co-doped Ti_2CO_2(NS) in Fig. 6. The PBE functional calculation for pristine Ti_2CO_2 yields a band gap of $E_{gap} = 0.25$ eV, which is consistent with the previous reported DFT values of 0.2–0.3 eV.[53,61–63] When applying the DFT + U correction, the band gap increases to $E_{gap} = 0.75$ eV, in good agreement with the range of 0.67–1.32 eV reported from DFT + U, GW, and HSE06 calculations.[49,50] From the PDOS, the valence states of Ti_2CO_2 consist of C 2p, Ti 3d, and O 2p orbitals. The hybridization of C 2p states plays the most significant role in the bonding region at −2 eV. Meanwhile, the Ti 3d orbitals are the dominant contributor to conducting states, and the valence peak is just below the Fermi level. Doping S or co-doping N and S atoms to the termination layer of Ti_2CO_2 causes the presence of outermost p-states from the doping element, which increases the PDOS of the VBM and CBM. Thus, the doped and codoped MXene express narrower band gaps, such as $E_{gap} = 0.31$ eV for Ti_2CO_2(S) and $E_{gap} = 0.26$ eV for co-doped Ti_2CO_2(NS). Moreover, the doped atom provides a higher DOS to the valence region near the Fermi level, and the Fermi level is shifted into the continuous density of states of the valence band. Both these effects improve the hole concentration, which elevates the electronic conductivity of our MXene. It is due to the highly polarized electron-rich doped atoms donating their electron to nearby Ti atoms, increasing the DOS of Ti 3d at the Fermi level. The similar effect of the doped N element is less than that of the doped S element in the co-doped scheme. Therefore, doping or co-doping heteroatoms on the surface of Ti_2CO_2 could be beneficial for electrochemical performance, as it would result in higher carrier mobility and electronic conductivity. Such behavior is consistent with other studies of S-doped $Ti_3C_2O_2$ MXene and graphene-based nanosheets.[26,34] DOS analysis based on DFT calculations of N,S-MXene[36] also demonstrated that the N,S co-doping could improve the electronic performance of MXene as it possesses better electrical conductivity to facilitate electron transfer. In the study of co-doped N and S on the surface of $Ti_3C_2T_x$ MXene. Herein, doped N and S atoms lead to more unfilled valencies for NS-MXene compared to undoped MXene. This point theoretically suggests that more redox capacity and larger capacitance could be achieved through N,S co-doping of MXene.[37]

Upon adsorption of sodium polysulfides, we analyze the electronic properties of doped Ti_2CO_2(S) and co-doped Ti_2CO_2(NS). The PDOS of these systems with Na_2S, Na_2S_4, and Na_2S_8 clusters are presented in Fig. 7 and 8. The introduction of Na and S states significantly enhances the DOS near the Fermi level in both doped systems, thereby improving electronic conductivity and supporting better electrochemical performance. The pronounced peak of S p-states at the Fermi level further contributes to enhanced conductivity. Notably, the co-
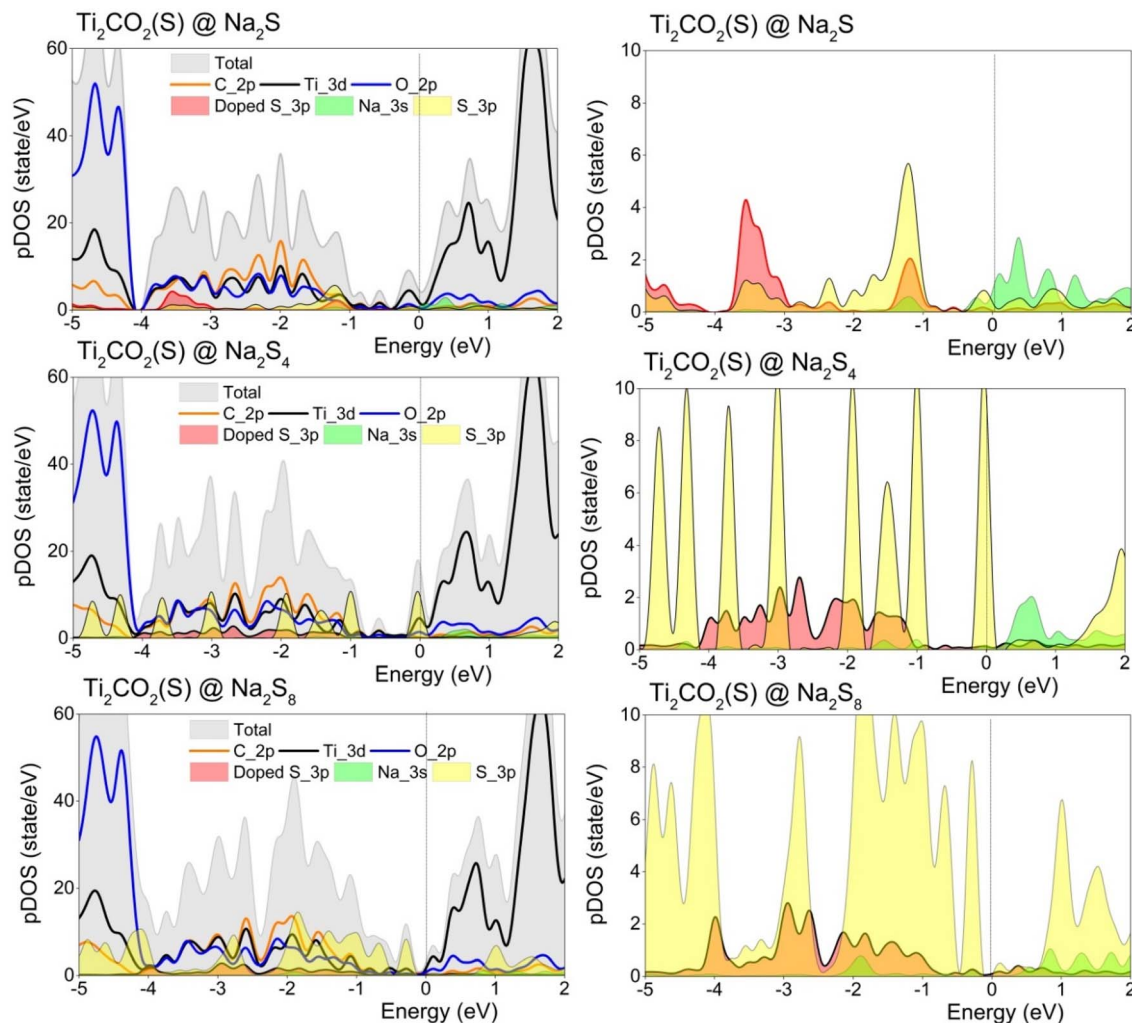
Fig. 7 Projected density of states of doped $Ti_2CO_2(S)$ upon adsorption of Na_2S, Na_2S_4, and Na_2S_8 clusters calculated by DFT + U (left), and enlarged PDOS of p-states of doped atom, Na s-state, and S s-state of Na_2S, Na_2S_4, and Na_2S_8 clusters (right). The Fermi level is set to zero and is indicated by the dashed lines.

doped $Ti_2CO_2(NS)$ exhibits a much higher total DOS compared to the singly doped $Ti_2CO_2(S)$, indicating superior electronic conductivity for polysulfide adsorption. Upon adsorption of Na–S clusters, the presence of Na and S states provides boosted DOS in the Fermi level in both doped $Ti_2CO_2(S)$ and co-doped $Ti_2-CO_2(NS)$, which enhances conductivity for electrochemical performance. The pronounced peak of p states of the S atom at the Fermi level promotes the electronic conductivity of our MXene. Therefore, we found that the co-doped $Ti_2CO_2(NS)$ offers better promotion of the electronic conductivity for our adsorption schemes as the total DOS is much increased compared to the doped $Ti_2CO_2(S)$.

For $Ti_2CO_2(S)$ in Fig. 7, the strongest adsorption of Na_2S observed in Fig. 4 can be attributed to strong hybridization between the p-states of the doped S atom and the orbitals of Na and S in the polysulfide cluster at the Fermi level and around −1.2 eV. However, for Na_2S_4 and Na_2S_8 clusters, the binding between the doped S atom and Na is weakened as

the Na s-orbitals shift toward lower energies. In contrast, for $Ti_2CO_2(NS)$ (Fig. 8), N,S co-doping facilitates stronger interactions between the p-states of both dopant atoms and the Na s-states, particularly for high sulfur-content clusters such as Na_2S_8.

A more detailed analysis of charge transfer of Na–S clusters and doped atoms is shown in Table 1. Compared to pristine MXene, the doped atom participates in a remarkable charge transfer, thereby increasing the charge migration between the MXene's surface and sodium polysulfide clusters. While S-doping is particularly effective for charge migration in low-S content clusters, such as Na_2S, this doping is less effective for higher S-content clusters, like Na_2S_8. By co-doping N atoms together with S atoms, the charge migration from higher S-content clusters, such as Na_2S_8, can be enhanced, resulting in a greater adsorption energy gain.

To further elucidate the charge transfer mechanism, we present the charge density difference (CDD) plots in Fig. 9,
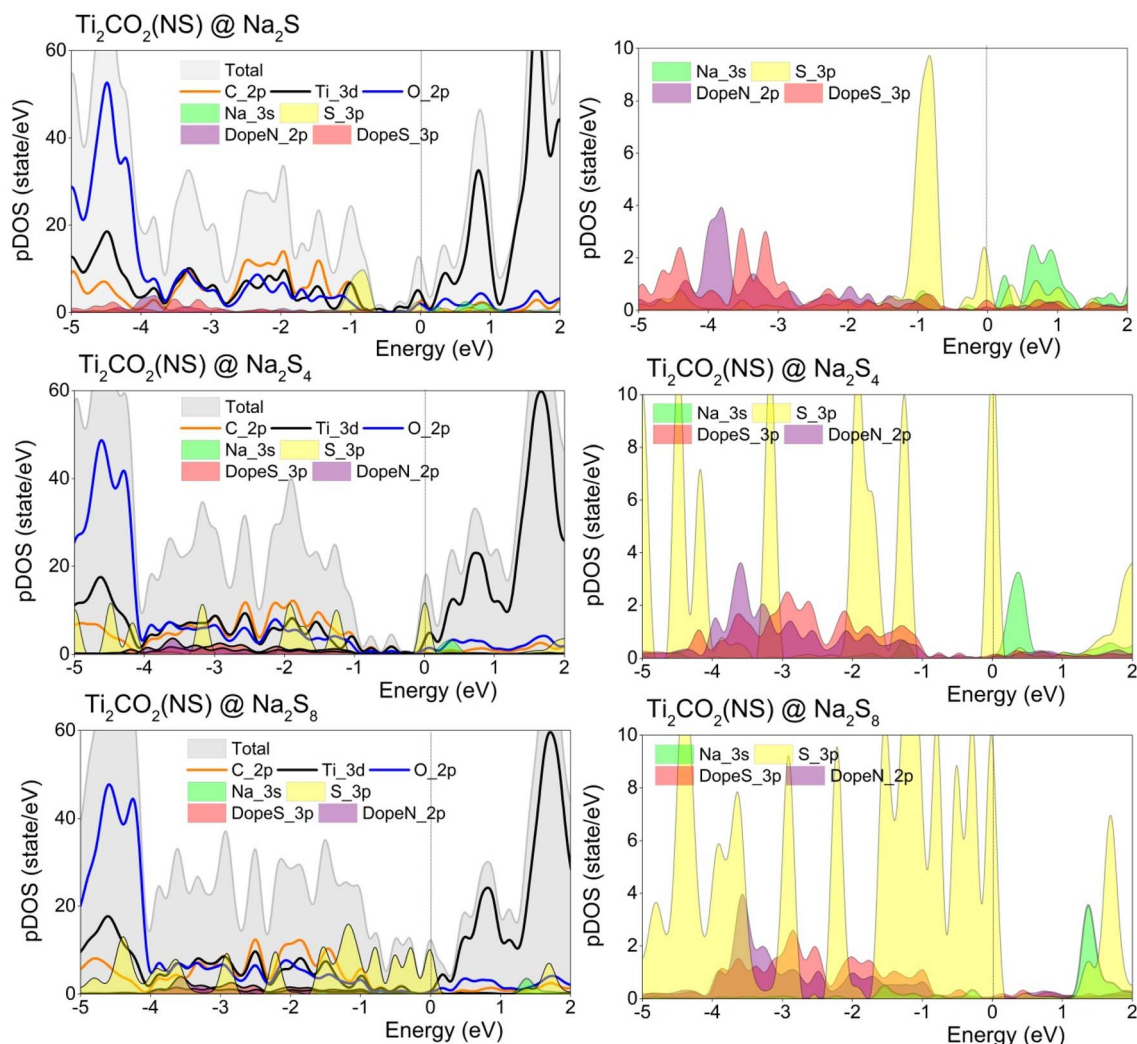
Fig. 8 Projected density of states of co-doped $Ti_2CO_2(NS)$ upon adsorption of Na_2S, Na_2S_4, and Na_2S_8 clusters calculated by DFT + U (left), and enlarged PDOS of p-states of doped atom, Na s-state, and S s-state of Na_2S, Na_2S_4, and Na_2S_8 clusters (right). The Fermi level is set to zero and is indicated by the dashed lines.

Table 1 Summation of Bader charge transferred for Na and S atoms for Na_2S, Na_2S_4, and Na_2S_8 clusters on pristine $Ti_2CO_2(S)$, doped $Ti_2CO_2(S)$, and co-doped $Ti_2CO_2(NS)$. These values of the Bader charge are computed as the difference between the Bader charge calculated for Na_2S_x clusters absorbed on MXenes and the pristine Na_2S_x molecules, as well as the doped atoms with and without the absorbed Na_2S_x clusters

MXene	Charge transfer	Na_2S	Na_2S_4	Na_2S_8
Pristine Ti_2CO_2	Na–S cluster	0.76	0.84	0.32
Doped $Ti_2CO_2(S)$	Na–S cluster	0.93	0.85	0.58
	Doped S	0.34	0.21	0.24
Co-doped $Ti_2CO_2(NS)$	Na–S cluster	0.81	0.91	0.84
	Doped S	0.30	0.15	0.25
	Doped N	0.19	0.20	0.35

where yellow and cyan iso-surfaces represent regions of charge accumulation and depletion, respectively. Upon adsorption of Na_2S_x clusters, the redistribution of charge reveals the pivotal

role of dopant atoms in mediating chemical interactions. In the case of S-doped Ti_2CO_2, the interaction with the Na_2S cluster is characterized by a notable charge migration originating from the doped sulfur atom. Conversely, in the N,S co-doped Ti_2CO_2 structure, the doped sulfur site exhibits charge depletion, while the nitrogen dopant shows charge accumulation, consistent with its higher electronegativity. These observations are in line with previous findings on N-doped MXenes, where both Li atoms and Li_2S clusters experience greater charge loss due to electron transfer toward the nitrogen dopant.[30] For the Na_2S_8 cluster, substantial charge redistribution is observed in both doped systems. However, $Ti_2CO_2(NS)$ displays enhanced charge transfer contributions from the p-states of the dopant atoms, particularly nitrogen. This indicates a stronger chemical interaction between the co-doped MXene and the high sulfur-content cluster, suggesting improved anchoring capability through synergistic charge transfer effects.
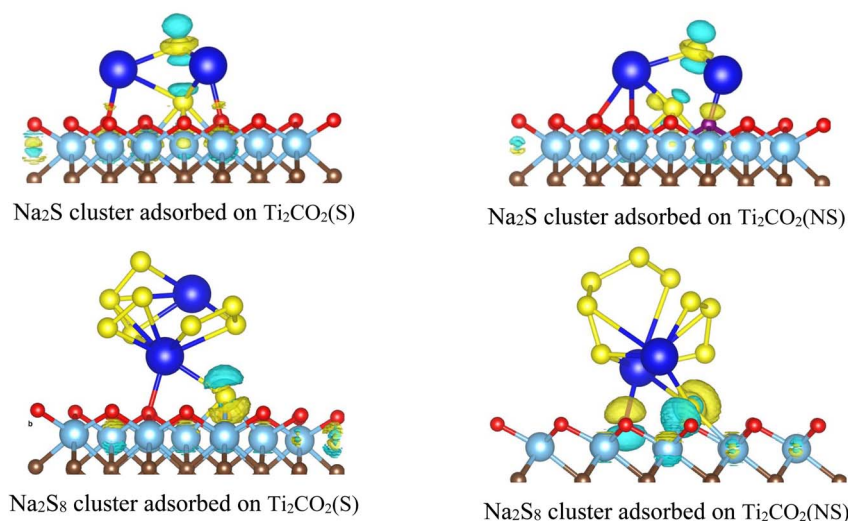
Fig. 9 Charge density difference (CDD) upon adsorption of low S-content (Na_2S) and high S-content (Na_2S_8) clusters on S-doped Ti_2CO_2 and NS co-doped Ti_2CO_2. The iso-surface is set at 0.01 e$Å^{-3}$. Yellow regions indicate charge accumulation, while cyan regions denote charge depletion.

Na$_2$S cluster adsorbed on Ti$_2$CO$_2$(S)

Na$_2$S cluster adsorbed on Ti$_2$CO$_2$(NS)

Na$_2$S$_8$ cluster adsorbed on Ti$_2$CO$_2$(S)

Na$_2$S$_8$ cluster adsorbed on Ti$_2$CO$_2$(NS)

4. Conclusions

In this study, we systematically investigated the role of sulfur doping (S-doped) and, more importantly, nitrogen-sulfur co-doping (NS co-doped) of Ti_2CO_2 MXene as anchoring materials for sodium polysulfide (Na_2S_x) clusters in sodium–sulfur (Na–S) batteries using first-principles calculations. Our results demonstrate that the introduction of NS co-dopants significantly enhances the adsorption strength toward Na_2S_x clusters compared to both pristine and solely S-doped Ti_2CO_2 MXenes. Particularly, NS co-doped Ti_2CO_2 exhibits superior binding capability toward high sulfur-content polysulfides (Na_2S_6 and Na_2S_8), which are typically challenging to anchor due to their strong tendency toward dissolution. The electronic structure analysis reveals that both S-doped and NS co-doped systems exhibit higher DOS in the valence region, thus substantially enhancing electronic conductivity, a critical factor for efficient electrochemical performance. Detailed charge transfer, charge density difference, and projected density of states analyses highlight strong hybridization between dopant p-states and Na s- and S p-states, confirming robust chemical interactions essential for polysulfide immobilization. These findings underline the remarkable advantages of S-doped and NS co-doped Ti_2CO_2 MXene as highly effective anchoring materials, emphasizing its potential to overcome existing challenges related to the shuttle effect and electrical conductivity in Na–S battery technology.

Conflicts of interest

There are no conflicts of interest to declare.

Data availability

The data supporting this article have been included as part of the SI. Supplementary information: structural optimized data for pristine Ti_2CO_2 MXene, S-doped Ti_2CO_2(S), and co-doped Ti_2CO_2(NS). See DOI: **https://doi.org/10.1039/d5ra05003k**.

References

1 J.-M. Tarascon and M. Armand, Issues and Challenges Facing Rechargeable Lithium Batteries, *Nature*, 2001, **414**, 359–367, DOI: **10.1038/35104644**.

2 S. Zhang, Y. Yao and Y. Yu, Frontiers for Room-Temperature Sodium–Sulfur Batteries, *ACS Energy Lett.*, 2021, **6**(2), 529–536, DOI: **10.1021/acsenergylett.0c02488**.

3 R. Fang, S. Zhao, Z. Sun, D.-W. Wang, H.-M. Cheng and F. Li, More Reliable Lithium-Sulfur Batteries: Status, Solutions and Prospects, *Adv. Mater.*, 2017, **29**(48), 1606823, DOI: **10.1002/adma.201606823**.

4 T. H. N. Thi, N. T. Van, M. T. Dang, N. V. A. Duy, T. S. Luong, S. D. Le, T. N. Van, D. L. Vu and N. N. Van, Co and F co-doping to augmenting the electrochemical performance of P2-type sodium lithium manganese oxide for sodium ion battery, *J. Electroanal. Chem.*, 2024, **972**, 118590, DOI: **10.1016/j.jelechem.2024.118590**.

5 H. Shen, D. Rao, X. Xi, Y. Liu and X. Shen, N-substituted defective graphene sheets: promising electrode materials for Na-ion batteries, *RSC Adv.*, 2015, **5**, 17042–17048, DOI: **10.1039/C4RA15010D**.

6 X. Lu, B. W. Kirby, W. Xu, G. Li, J. Y. Kim, J. P. Lemmon, V. L. Sprenkle and Z. Yang, Advanced Intermediate-Temperature Na–S Battery, *Energy Environ. Sci.*, 2013, **6**, 299–306, DOI: **10.1039/C2EE23606K**.

7 X. Zhou, D. Qin, X. Lin, K. Kang, F. Li, B. Shanmukaraj, T. Rojo, M. Armand and G. Wang, A room-temperature sodium–sulfur battery with high capacity and stable cycling performance, *Nat. Commun.*, 2018, **9**, 3870, DOI: **10.1038/s41467-018-06443-3**.

8 Y. Wang, R. Chen, T. Chen, H. Lv, G. Zhu, L. Ma, C. Wang, Z. Jin and J. Liu, Emerging non-lithium ion batteries,

Energy Storage Mater., 2016, **4**, 103–129, DOI: **10.1016/j.ensm.2016.04.001**.

9 R. Jayan and M. M. Islam, Single-atom catalysts for improved cathode performance in Na–S batteries: a density functional theory (DFT) study, *J. Phys. Chem. C*, 2021, **125**, 4458–4467, DOI: **10.1021/acs.jpcc.1c00467**.

10 M. K. Aslam, Y. Niu and M. Xu, MXenes for non-lithium-ion (Na, K, Ca, Mg, and Al) batteries and supercapacitors, *Adv. Energy Mater.*, 2021, **11**, 2000681, DOI: **10.1002/aenm.202000681**.

11 P. Hartmann, C. L. Bender, M. Busche, C. Eufinger, J. Janek and P. Adelhelm, From lithium to sodium: cell chemistry of room temperature sodium-air and sodium-sulfur batteries, *Beilstein J. Nanotechnol.*, 2015, **6**, 1016–1055, DOI: **10.3762/bjnano.6.105**.

12 N. Thatsami, P. Tangpakonsab, P. Moontragoon, R. Umer, T. Hussain and T. Kaewmaraya, Two-dimensional titanium carbide ($Ti_3C_2T_x$) MXenes to inhibit the shuttle effect in sodium sulfur batteries, *Phys. Chem. Chem. Phys.*, 2022, **24**, 4187–4195, DOI: **10.1039/D1CP05300K.**

13 T.-T. Yu, P.-F. Gao, Y. Zhang and S.-L. Zhang, Boron-phosphide monolayer as a potential anchoring material for lithium-sulfur batteries: a first-principles study, *Appl. Surf. Sci.*, 2019, **486**, 281–286, DOI: **10.1016/j.apsusc.2019.05.019**.

14 Z. Xiang, Y. Li, Y. Gao, Z. Wang and L. Chen, Theoretical exploration of the structural evolution of sodium sulfide clusters in Na–S batteries, *Appl. Surf. Sci.*, 2023, **613**, 155906, DOI: **10.1016/j.apsusc.2022.155906**.

15 Y.-X. Wang, Z. Sun, Y.-G. Guo and L.-J. Wan, Achieving high-performance room-temperature sodium–sulfur batteries with S@interconnected mesoporous carbon hollow nanospheres, *J. Am. Chem. Soc.*, 2016, **138**(51), 16576–16579, DOI: **10.1021/jacs.6b08685**.

16 R. Jayan and M. M. Islam, Mechanistic insights into interactions of polysulfides at VS_2 interfaces in Na–S batteries: a DFT study, *ACS Appl. Mater. Interfaces*, 2021, **13**, 35848–35855, DOI: **10.1021/acsami.1c10868**.

17 T. Kaewmaraya, T. Hussain, R. Umer, Z. Hu and X. S. Zhao, Efficient suppression of the shuttle effect in Na–S batteries with an As_2S_3 anchoring monolayer, *Phys. Chem. Chem. Phys.*, 2020, **22**, 27300–27307, DOI: **10.1039/D0CP05507G**.

18 J. Li, S. Guan, L. Pan, Z. Li, G. Ji, J. Pan and X. Xu, MXene-based anode materials for high performance sodium-ion batteries, *J. Colloid Interface Sci.*, 2024, **658**, 425–440, DOI: **10.1016/j.jcis.2023.12.065**.

19 L. Zhang and Y. Hou, MXenes: synthesis strategies and lithium-sulfur battery applications, *eScience*, 2022, **2**, 164–182, DOI: **10.1016/j.esci.2022.02.010**.

20 J. Chattopadhyay, T. S. Pathak and D. M. F. Santos, Applications of polymer electrolytes in lithium-ion batteries: a review, *Polymers*, 2023, **15**, 4394, DOI: **10.3390/polym15193907**.

21 N. T. Long, N. T. Phung, V. B. T. Trang, N. T. A. Nguyen, T. N. Tran, N. V. A. Duy, N. T. Van, N. Van Nghia and P. Schall, Resolving adsorption mechanism of sodium polysulfides on $Ti_{m+1}C_mO_2$ MXenes for application in sodium–sulfur batteries: a first-principles study, *Appl. Surf. Sci.*, 2025, **687**, 162210, DOI: **10.1016/j.apsusc.2024.162210**.

22 Z. Chang, Z. Liu and N. Zhou, Functionalized M_2CT_2 (M = Ti, V, Cr, Mn; T = O, Chen and S, Se) MXenes as anchoring materials for lithium–sulfur batteries, *Appl. Surf. Sci.*, 2022, **602**, 154375, DOI: **10.1016/j.apsusc.2022.154375**.

23 H. Wang, A. de Kogel, Z. Wang, R. Zou and X. Wang, Strategies of tailoring 2D MXenes for enhancing sulfur-based battery performance, *Chem. Eng. J.*, 2025, **459**, 159924, DOI: **10.1016/j.cej.2025.159924**.

24 B. Gong, X. Shi, Y. Liu and J. Hao, Understanding the inhibition of the shuttle effect of sulfides (S≤3) in lithium–sulfur batteries by heteroatom-doped graphene: first-principles study, *J. Phys. Chem. C*, 2020, **124**, 6, DOI: **10.1021/acs.jpcc.9b10314**.

25 J. Shen, Z. Wang, X. Xu, Z. Liu, D. Zhang, F. Li, Y. Li, L. Zeng and J. Liu, Surface/interface structure and chemistry of lithium–sulfur batteries: from density functional theory calculations' perspective, *Adv. Energy Sustain. Res.*, 2021, **2**, 2100007, DOI: **10.1002/aesr.202100007**.

26 Y. Ma, X. Ning, G. Wang, Y. Song, X. Xiao, Z. Hou, L. Yang, W. Gao and J. Li, S-doped mesoporous graphene microspheres: a high performance reservoir material for Li–S batteries, *Electrochim. Acta*, 2018, **269**, 83–92, DOI: **10.1016/j.electacta.2018.02.163**.

27 Y. Wen, T. E. Rufford, X. Chen, N. Li, M. Lyu, L. Dai and L. Wang, Nitrogen-doped $Ti_3C_2T_x$ MXene electrodes for high-performance supercapacitors, *Nano Energy*, 2017, **38**, 368–376, DOI: **10.1016/j.nanoen.2017.06.009**.

28 S. Sun, B. Hua, B. Shi, J. Xu and Z. Peng, First-principles study on the electronic, magnetic, and Li-ion mobility properties of N-doped Ti_2CO_2, *Solid State Ionics*, 2022, **383**, 115983, DOI: **10.1016/j.ssi.2022.115983**.

29 J. Li, Y. Zhang, W. Chen, L. Wang, J. Liu and H. Zhao, MXene-based anode materials for high performance sodium-ion batteries, *J. Colloid Interface Sci.*, 2024, **658**, 425–440, DOI: **10.1016/j.jcis.2023.12.065**.

30 Y. Song, Z. Sun, Z. Fan, W. Cai, Y. Shao, G. Sheng, M. Wang, L. Song, Z. Liu, Q. Zhang and J. Sun, Rational design of porous nitrogen-doped Ti_3C_2 MXene as a multifunctional electrocatalyst for Li–S chemistry, *Nano Energy*, 2020, **70**, 104555, DOI: **10.1016/j.nanoen.2020.104555**.

31 J. Zhang, X. Yan, S. Zhang, Z. Wu, Z. Zhuang and W. Q. Han, Rational design of porous $N-Ti_3C_2$ MXene@CNT microspheres for high cycling stability in Li–S battery, *Nano-Micro Lett.*, 2020, **12**, 45, DOI: **10.1007/s40820-019-0341-6**.

32 W. Bao, C. E. Shuck, W. Zhang, X. Guo, Y. Gogotsi and G. Wang, Boosting performance of Na–S batteries using sulfur-doped $Ti_3C_2T_x$ MXene nanosheets with a strong affinity to sodium polysulfides, *ACS Nano*, 2019, **13**, 11500–11509, DOI: **10.1021/acsnano.9b04977**.

33 Y. Yuan, J. Yang and Y. W. Zhang, S-doped $Ti_3C_2F_2$ MXene as an ideal sulfur cathode host for high-performance rechargeable lithium–sulfur batteries, *J. Mater. Chem. A*, 2023, **11**, 17841–17847, DOI: **10.1039/D3TA03518B**.

34 P. Komen, L. Ngamwongwan, S. Jungthawan, A. Junkaew and S. Suthirakun, Promoting electrochemical performance of $Ti_3C_2O_2$ MXene-based electrodes of alkali-ion batteries via S doping: theoretical insight, *ACS Appl. Mater. Interfaces*, 2021, **13**, 57306–57316, DOI: **10.1021/acsami.1c17802**.

35 Y. Li, J. Yan, D. Hou, S. Li, Y. Lu, Y. Yao and L. Pan, Improved sodium-ion storage performance of $Ti_3C_2T_x$ MXenes by sulfur doping, *J. Mater. Chem. A*, 2018, **6**, 1234–1243, DOI: **10.1039/C7TA08261D**.

36 P. Sun, J. Liu, Q. Liu, J. Yu, R. Chen, J. Zhu, G. Sun, Y. Li, P. Liu and J. Wang, Nitrogen and sulfur co-doped MXene ink without additive for high-performance inkjet-printing micro-supercapacitors, *Chem. Eng. J.*, 2022, **450**, 138372, DOI: **10.1016/j.cej.2022.138372**.

37 F. Yang, D. Hegh, D. Song, J. Zhang, K. A. S. Usman, C. Liu, Z. Wang, W. Ma, W. Yang, S. Qin and J. M. Razal, Synthesis of nitrogen-sulfur co-doped $Ti_3C_2T_x$ MXene with enhanced electrochemical properties, *Mater. Rep. Energy*, 2022, **2**, 100079, DOI: **10.1016/j.matre.2022.100079**.

38 R. Cheng, T. Hu, J. Yang, Z. Wang, W. Wang, Y. Liang, Z. Yang, H. Zhang and X. Wang, Nitrogen and sulfur co-doped $Ti_3C_2T_x$ MXenes for high-rate lithium-ion batteries, *Phys. Chem. Chem. Phys.*, 2023, **25**, 10635–10646, DOI: **10.1088/1361-648X/aa8f79**.

39 P. Giannozzi, O. Baseggio, P. Bonfà, D. Brunato, R. Car, I. Carnimeo, C. Cavazzoni, S. de Gironcoli, P. Delugas, F. Ferrari Ruffino, A. Ferretti, N. Marzari, I. Timrov, A. Urru and S. Baroni, Advanced capabilities for materials modelling with Quantum ESPRESSO, *J. Phys.: Condens. Matter*, 2017, **29**, 465901, DOI: **10.1088/1361-648X/aa8f79**.

40 P. E. Blöchl, Projector augmented-wave method, *Phys. Rev. B: Condens. Matter Mater. Phys.*, 1994, **50**, 17953, DOI: **10.1103/PhysRevB.50.17953**.

41 J. P. Perdew, K. Burke and M. Ernzerhof, Generalized Gradient Approximation Made Simple, *Phys. Rev. Lett.*, 1996, **77**, 3865–3868, DOI: **10.1103/PhysRevLett.77.3865**.

42 A. Dal Corso, Pseudopotentials periodic table: From H to Pu, *Comput. Mater. Sci.*, 2014, **95**, 337–350, DOI: **10.1016/j.commatsci.2014.07.043**.

43 K. Lee, É. D. Murray, L. Kong, B. I. Lundqvist and D. C. Langreth, Higher-accuracy van der Waals density functional, *Phys. Rev. B: Condens. Matter Mater. Phys.*, 2010, **82**, 081101, DOI: **10.1103/PhysRevB.82.081101**.

44 D. Chakraborty, K. Berland and T. Thonhauser, Next-generation nonlocal van der Waals density functional, *J. Chem. Theory Comput.*, 2020, **16**, 5893–5911, DOI: **10.1021/acs.jctc.0c00471**.

45 H. J. Monkhorst and J. D. Pack, Special points for Brillouin-zone integrations, *Phys. Rev. B: Condens. Matter Mater. Phys.*, 1976, **13**, 5188–5192, DOI: **10.1103/PhysRevB.13.5188**.

46 V. I. Anisimov, J. Zaanen and O. K. Andersen, Band theory and Mott insulators: Hubbard U instead of Stoner I, *Phys. Rev. B: Condens. Matter Mater. Phys.*, 1991, **44**, 943, DOI: **10.1103/PhysRevB.44.94**.

47 V. L. Campo Jr and M. Cococcioni, Extended DFT+U+V method with on-site and inter-site electronic interactions, *J. Phys.: Condens. Matter*, 2010, **22**, 055602, DOI: **10.1088/0953-8984/22/5/055602**.

48 I. Timrov, N. Marzari and M. Cococcioni, Self-consistent Hubbard parameters from density-functional perturbation theory in the ultrasoft and projector-augmented wave formulations, *Phys. Rev. B*, 2021, **103**, 045141, DOI: **10.1103/PhysRevB.103.045141**.

49 T. Sakhraoui and F. Karlický, Electronic Nature Transition and Magnetism Creation in Vacancy-Defected Ti_2CO_2 MXene under Biaxial Strain: A DFTB + U Study, *ACS Omega*, 2022, **7**, 42221–42232, DOI: **10.1021/acsomega.2c05037**.

50 T. Wang, N. Li, Y. Li, J.-J. Kai and J. Fan, M-Site Vacancy-Mediated Adsorption and Diffusion of Sodium on Ti_2CO_2 MXene, *J. Phys. Chem. C*, 2021, **125**, 82–90, DOI: **10.1021/acs.jpcc.0c08302**.

51 C. Wang, H. Han and Y. Guo, Stabilities and electronic properties of vacancy-doped Ti_2CO_2, *Comput. Mater. Sci.*, 2019, **159**, 127–135, DOI: **10.1016/j.commatsci.2018.12.007**.

52 A. Bafekry, M. M. Fadlallah, F. Molaei, N. N. Hieu, P. Qian, M. Ghergherehchi and D. Gogova, Surface modification of titanium carbide MXene monolayers (Ti_2C and Ti_3C_2) via chalcogenide and halogenide atoms, *Phys. Chem. Chem. Phys.*, 2021, **23**, 23745–23757, DOI: **10.1039/D1CP01788H**.

53 X. H. Zhang, K. Luo, N. Qiu, Y. Zhou, J. He, Z. Chai, Z. Huang, Q. Huang, Y. Liang and S. Du, Tuning the electrical conductivity of Ti_2CO_2 MXene by varying the layer thickness and applying strains, *J. Phys. Chem. C*, 2019, **123**, 6802–6810, DOI: **10.1021/acs.jpcc.8b10888**.

54 W. Tang, E. Sanville and G. Henkelman, A grid-based Bader analysis algorithm without lattice bias, *J. Phys.: Condens. Matter*, 2009, **21**, 084204, DOI: **10.1088/0953-8984/21/8/084204**.

55 A. Otero-de-la-Roza, E. R. Johnson and V. Luaña, Critic2: A program for real-space analysis of quantum chemical interactions in solids, *Comput. Phys. Commun.*, 2014, **185**, 1007–1018, DOI: **10.1016/j.cpc.2013.10.026**.

56 M. S. Nahian, R. Jayan, T. Kaewmaraya, T. Hussain and M. M. Islam, Elucidating synergistic mechanisms of adsorption and electrocatalysis of polysulfides on double-transition metal MXenes for Na–S batteries, *ACS Appl. Mater. Interfaces*, 2022, **14**(8), 10298–10307, DOI: **10.1021/acsami.1c22511**.

57 N. Li, Y. Zhan, H. Wu, J. Fan and J. Jia, Covalent surface modification of bifunctional two-dimensional metal carbide MXenes as sulfur hosts for sodium–sulfur batteries, *Nanoscale*, 2022, **14**, 17027–17035, DOI: **10.1039/D2NR03462J**.

58 R. Jayan and M. M. Islam, First-Principles investigation of the anchoring behavior of pristine and defect-engineered tungsten disulfide for lithium–sulfur batteries, *J. Phys. Chem. C*, 2020, **124**, 27323–27332, DOI: **10.1021/acs.jpcc.0c08170**.

59 J. Li, Y. Qu, C. Chen, X. Zhang and M. Shao, Theoretical investigation on lithium polysulfide adsorption and conversion for high-performance Li–S batteries, *Nanoscale*, 2021, **13**, 15–35, DOI: **10.1039/D0NR06732F**.

60 Z. Yi, F. Su, L. Huo, G. Cui, C. Zhang, P. Han, N. Dong and C. Chen, New insights into Li_2S_2/Li_2S adsorption on the graphene bearing single vacancy: A DFT study, *Appl. Surf. Sci.*, 2020, **503**, 144446, DOI: 10.1016/j.apsusc.2019.144446.

61 Q. Zhou, L. Wang, W. Ju, Z. Zhao, J. Hou, Y. Yong and H. Miao, Effect of doping on the sensitivity of Ti_2CO_2 toward NO: A DFT study, *Phys. Lett. A*, 2023, **477**, 128919, DOI: 10.1016/j.physleta.2023.128919.

62 X. H. Li, S. S. Li, X. H. Cui, R. Z. Zhang and H. L. Cui, First-principle study of electronic properties and quantum capacitance of lithium adsorption on pristine and vacancy-defected O-functionalized Ti_2C MXene, *Appl. Surf. Sci.*, 2021, **563**, 150264, DOI: 10.1016/j.apsusc.2021.150264.

63 X. Gao, Y. Zhou, Y. Tan, Z. Cheng, B. Yang, Y. Ma, Z. Shen and J. Jia, Exploring adsorption behavior and oxidation mechanism of mercury on monolayer Ti_2CO_2 (MXenes) from first principles, *Appl. Surf. Sci.*, 2019, **464**, 53–60, DOI: 10.1016/j.apsusc.2018.09.071.